Supporting Materials

FeMnC complex derived from hollow FeMn PBA precursor for highly efficient microwave absorption

Peng Miao,[*a,c] Weixing Chen,[a] Dong Zhou,[b] Keji Zhu,[a] Jianing Zhang,[a] and Jie Kong [b]

[a] School of Materials and Chemical Engineering, Xi'an Technological University, Xi'an, Shaanxi, 710021, China.

[b] School of Chemistry and Chemical Engineering, Northwestern Polytechnical University, Xi'an, Shaanxi, 710072, China.

[c] Shaanxi Key Laboratory of Artificially-Structured Functional Materials and Devices, Xi'an, Shaanxi, 710043, China.

*Corresponding Author, E-mail Address: miaopeng@xatu.edu.cn

Experimental Section

Materials

All chemical reagents were brought commercially and used without further purification. Potassium ferrocyanide ($K_3[Fe(CN)_6]$) and manganese nitrate tetrahydrate ($Mn(NO)_3{\cdot}4H_2O$) were purchased from Macklin Corp. Sodium citrate ($C_6H_5Na_3O_7$) and polymethyl pyrrolidone (PVP, C_5H_9NO, K30, Da=40000) were obtained from Aladdin Corp., ethyl alcohol (C_2H_5OH, AR$\geqslant$98.5%) was brought from GHTECH Corp. The deionized (DI) water was fabricated in Lab.

Material synthesis

Synthesis of hollow Fe-Mn PBA precursor. The as-synthesized hollow Fe-Mn PBA precursors were prepared via a high-efficient coprecipitation and hydrothermal reaction process using a previous synthetic method.[1] Typically, 0.05 mmol of $K_3[Fe(CN)_6]$ is dissolved in 10 mL of DI water and stirred till a yellow transparent solution A; and 0.15 mmol of $Mn(NO)_3{\cdot}4H_2O$, 0.001 mmol of sodium citrate, and 2.0 g of PVP are dissolved in 35 mL of DI water and stirred till a transparent solution B. Then the solution B drops in the solution A in 30 seconds and which forms a dark brown solution C and stirring for 10 mins. Finally, transfer solution C to the oven ageing at 80 °C for 6 hours and a mixture of upper and lower layers in the beaker formed, and filter the upper solution and clean it serval times using ethyl alcohol.

Hollow FeMn PBA precursors derived FeMnC complex. The as-prepared hollow Fe-Mn PBA boxes were placed on the high-temperature resistant ceramic cup and transferred into a tube furnace (OTF-1200X, Kejing New Mater. Ltd., Hefei, China). The FeMnC complex was obtained by setting the stepwise heating process with a heating rate of 2 °C/min, and was kept at 500-800 °C under an argon atmosphere. The pyrolytic product can be obtained after with a fall rate of 5 °C/min.

Materials Characterization. The powder X-ray diffraction (PXRD) data of hollow FeMn PBA precursors was collected by a Rigaku-UltimaIV diffractometer using monochromatized Cu Kα radiation (Kα1, λ=1.540593 Å) flux at a scanning rate of 10 ˚min^{-1}. The thermogravimetric analysis (TGA) was conducted on a simultaneous thermal device (STA, 449 Jupiter, Netsch, Gerätebau GmbH, Selb, Germany) under a heating rate of 10 ˚min^{-1} from 40 to 1200 ˚C (Argon, 40 mL min^{-1}). The morphology and microstructure were observed using a field scanning electron microscopy (FESEM, FEI, Verios G4) and high-resolution transmission electron microscope (TEM, FEI, Talos F200X)

equipped with a selected area electron diffraction (SAED). The chemical composition and valence state were scanned by X-ray photoelectron spectroscopy (XPS) on a Kratos Axis Ultra DLD equipped with Al Kα radiation ($h\nu$=1486.6 eV) with a scanning voltage of 15 kV, and a scanning current of 10 mA. The magnetic response was surveyed by hysteresis loop using a physical property measurement system (Quantum Design, PPMS, Cryogenic, CFMS-14T).

Electromagnetic parameters measurement. The electromagnetic parameters of the FeMnC complex were collected by a vector network analyzer (VNA, Anritsu, MS46322B) using the coaxial transmission line method. The complex (microwave absorbers: paraffin=1:2, *wt*.%) was pressed into a coaxial ring with an outer diameter (Φ_o) of 7.00 mm and an inner diameter (Φ_i) of 3.04 mm in 2-18 GHz. The reflection loss (*RL*) is calculated by the following equation.

$$Z_{in} = \sqrt{\frac{\mu_r}{\varepsilon_r}} \tanh\left[j\frac{2\pi fd}{c}\sqrt{\mu_r \varepsilon_r} \right] \quad (1)$$

$$RL = 20\log_{10}\left|\frac{Z_{in}-1}{Z_{in}+1}\right| \quad (2)$$

$$\left(\varepsilon' - \frac{\varepsilon_s + \varepsilon_\infty}{2}\right) + (\varepsilon')^2 = \left(\frac{\varepsilon_s - \varepsilon_\infty}{2}\right)^2 \quad (3)$$

$$\alpha = \frac{\sqrt{2}\pi f}{c} \times \sqrt{(\mu''\varepsilon'' - \mu'\varepsilon') + \sqrt{(\mu''\varepsilon'' - \mu'\varepsilon')^2 + (\mu''\varepsilon' - \mu'\varepsilon'')^2}} \quad (4)$$

Where Z_{in}, μ_r, and ε_r are the normalized input impedance, permittivity, and permeability of the paraffined-based complex, respectively. The *f*, *d*, and *c* represent the microwave frequency, matching the thickness (*m*) of the sample and the velocity of the microwave in a vacuum, respectively. The ε_s and ε_∞ are the static permittivity and relative permittivity.

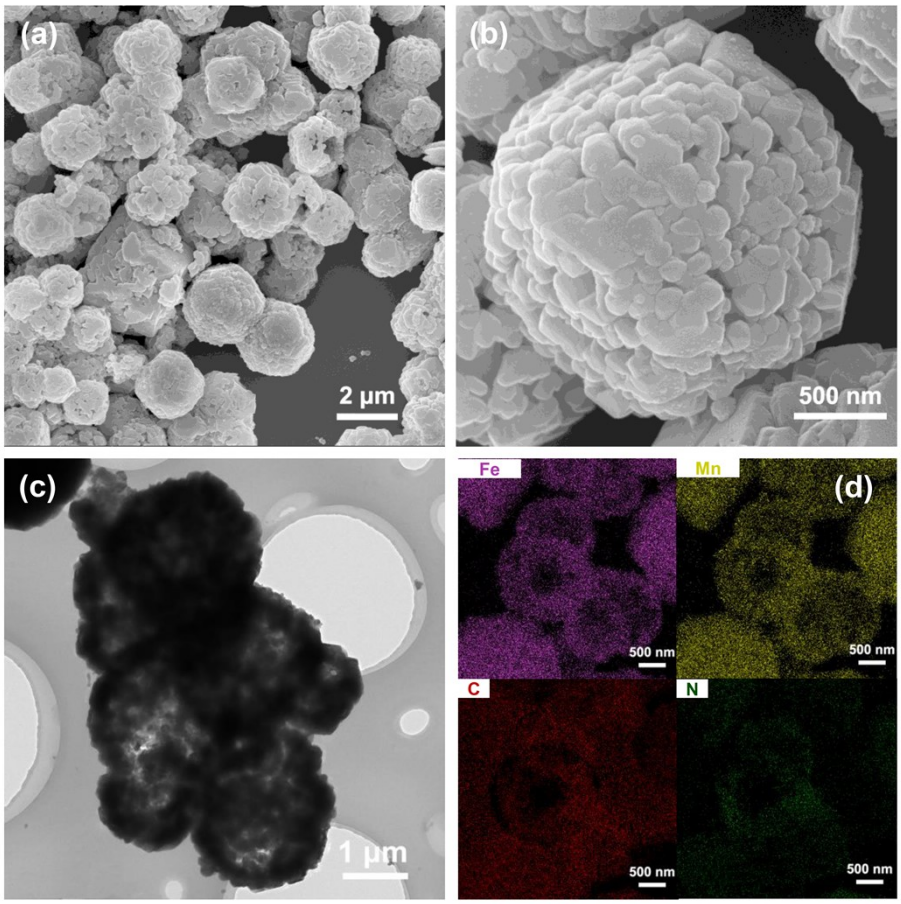

Figure S1 The microstructure of hollow Fe-Mn PBA precursors. (a) The SEM image, (b) magnifying SEM image, (c) TEM image, and (d) elemental mapping of Fe, Mn, C, and N.

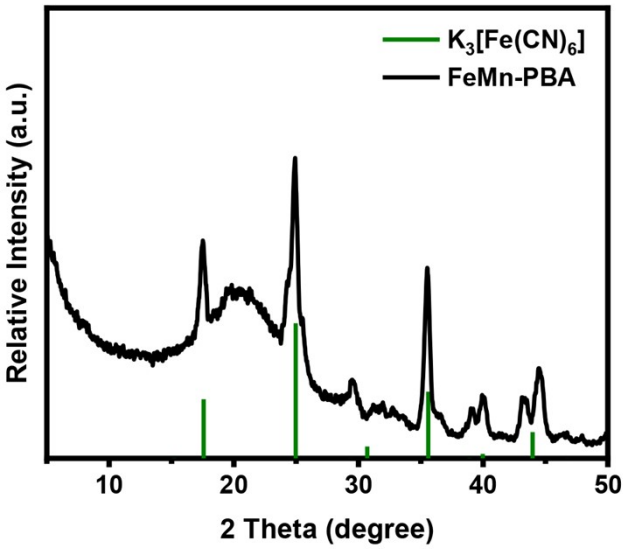

Figure S2 The phase composition of as-synthesized hollow Fe-Mn PBA precursors. The PXRD pattern.

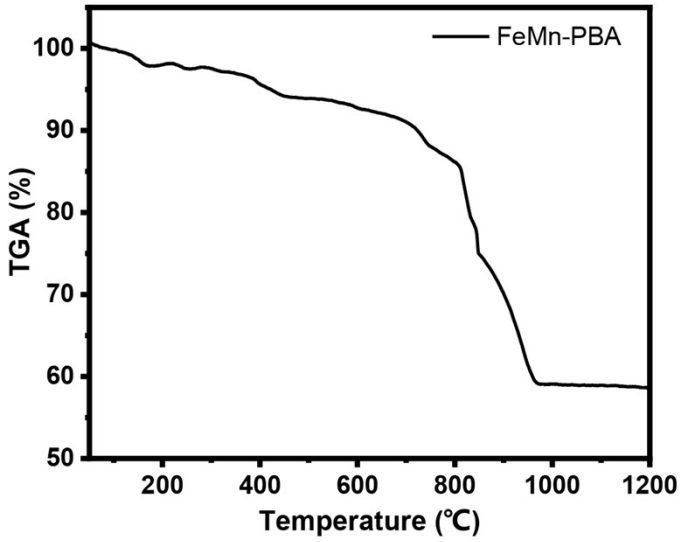

Figure S3 The thermal stability of as-synthesized hollow Fe-Mn PBA precursors. TGA curve.

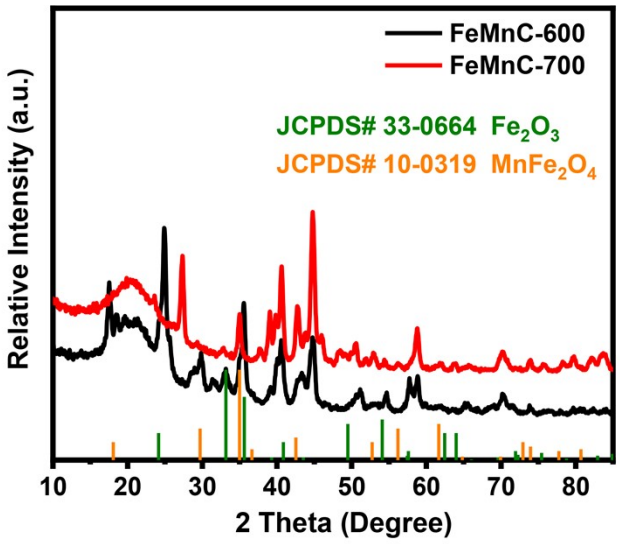

Figure S4 The powder X-ray diffraction (PXRD) patterns of the FeMnC-600 and FeMnC-700.

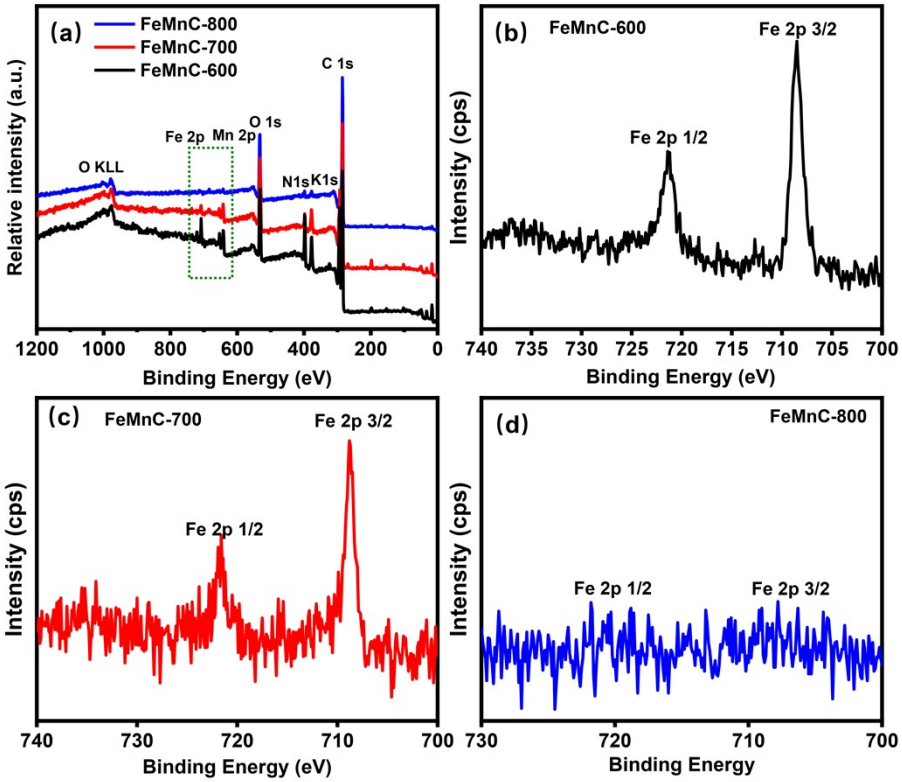

Figure S5 The chemical composition and valence state of iron for the FeMnC complex. (a) Survey spectra of FeMnC-600, FeMnC-700, and FeMnC-800, Narrow spectra of Fe element for (b) FeMnC-600, (c) FeMnC-700, (d) FeMnC-800.

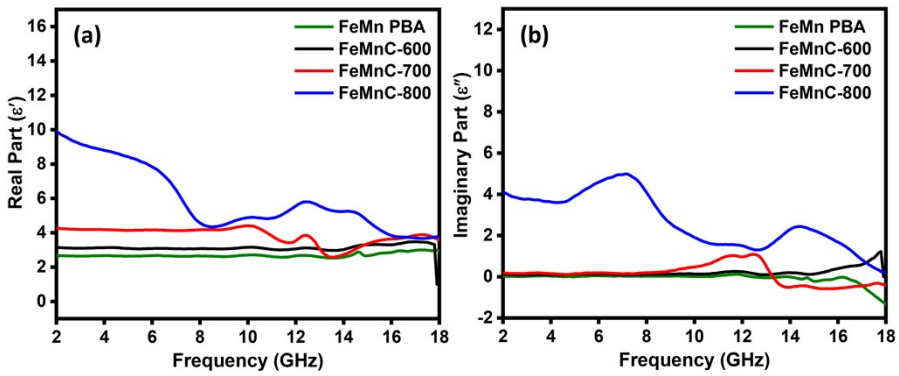

Figure S6 (a) Real parts (ε') and (b) imaginary parts (ε'') of complex permittivity of FeMn PBA, FeMnC-600, FeMnC-700, and FeMnC-800.

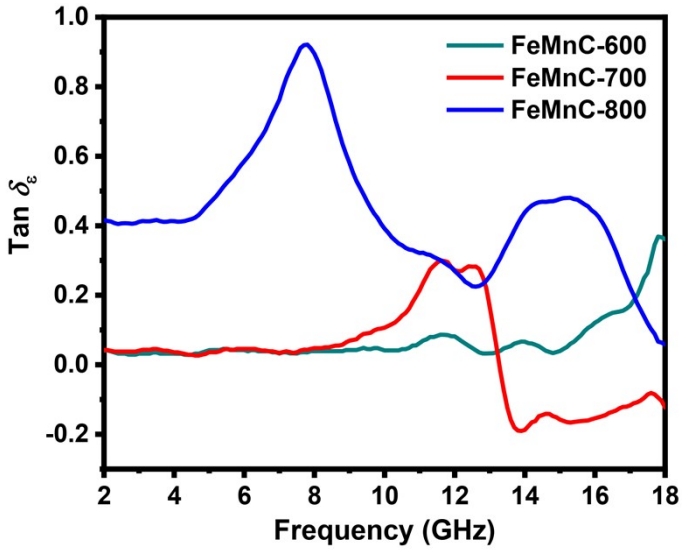

Figure S7 The tangent value of FeMnC complex with different pyrolysis temperatures (600, 700, and 800 °C)

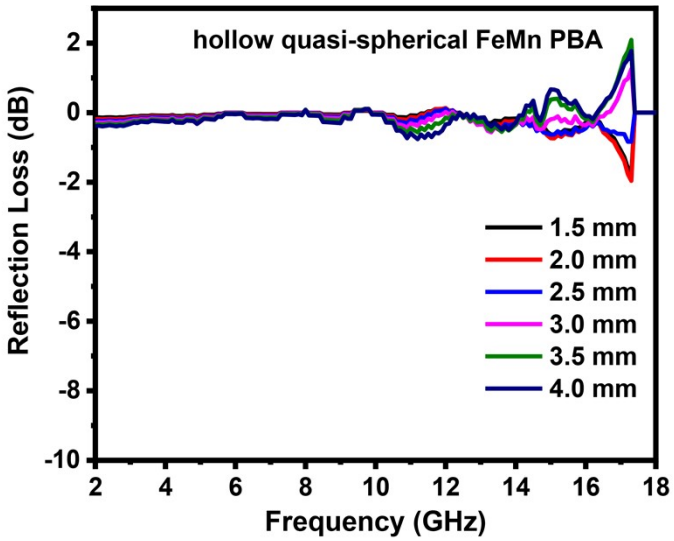

Figure S8 Reflection loss curves of hollow FeMn PBA precursors.

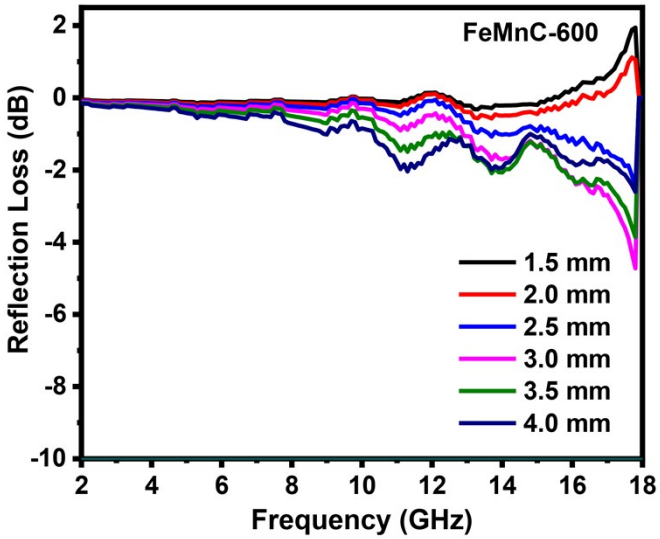

Figure S9 The reflection loss curves of the FeMnC complexes derived from hollow FeMn Prussian blue analogue (PBA) pyrolyzed at 600 ^{o}C.

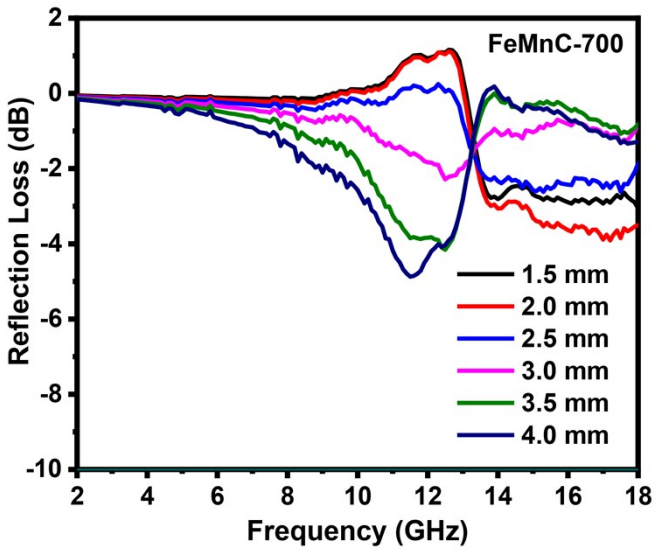

Figure S10 The reflection loss curves of the FeMnC complexes derived from hollow FeMn Prussian blue analogue (PBA) pyrolyzed at 700 ^{o}C.

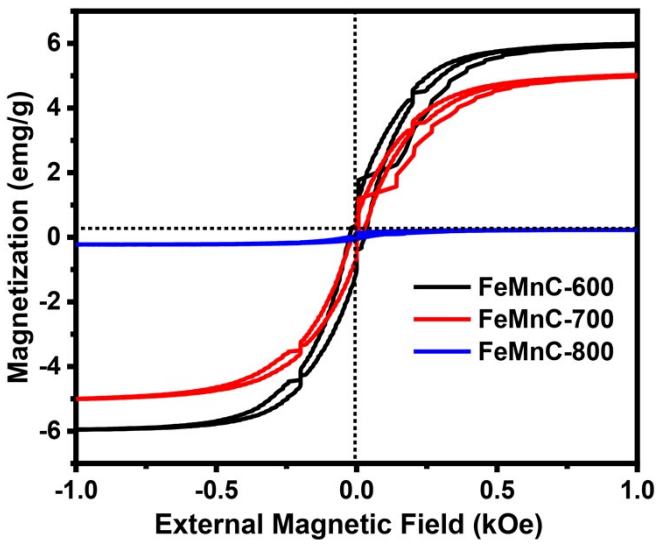

Figure S11 The hysteresis loops of the FeMnC complex with different pyrolysis temperatures (600, 700, and 800 °C)

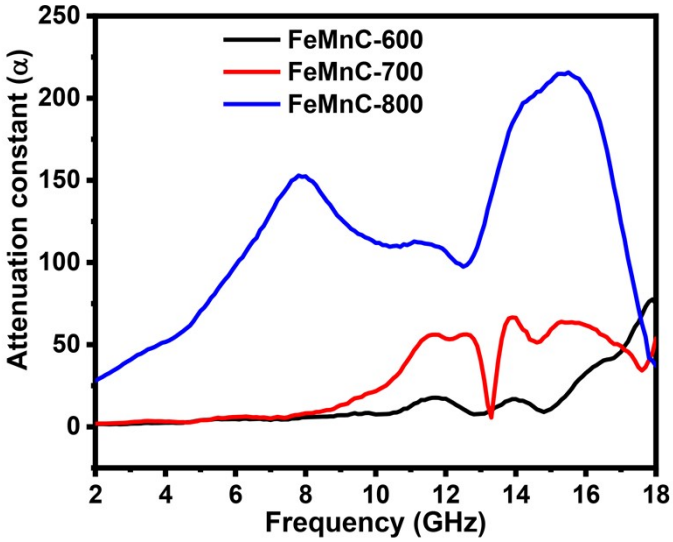

Figure S12 The microwave attenuation constant (α) of the FeMnC complex with different pyrolysis temperatures (600, 700, and 800°C).

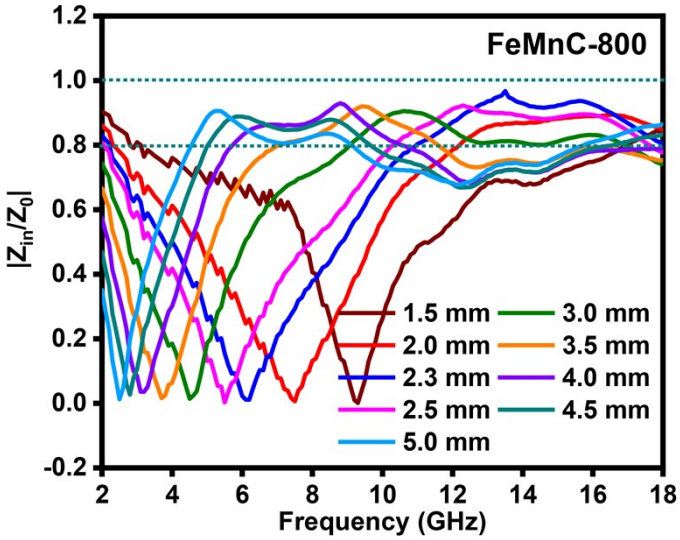

Figure S13 The normalized input impedance of the FeMnC-800.

Table S1 The microwave absorption properties of previously reported PBA-deriving complex as microwave absorbents.

Absorbers	Optimal thickness (mm)	Optimal RL (dB)	Effective absorption bandwidth (<-10 dB)		Loading/ *wt%*	Ref.
			thickness (mm)	EAB (GHz)		
CoNi@graphite@carbon	2.0	-56.78	2.0	5.51	30	2
CoAl/CoFe-CoCx@NC	3.8	-82.1	2.4	5.6	50	3
Fe/C (PB)	2.0	-20.3	2.0	7.2	40	4
FeCo Alloy	2.0	-33	1.5	4.6	40	5
Core-shell FeCo@carbon	2.0	-67.8	2.0	5.3	50	6
hollow NiCo@C	2.14	-68.4	2.0	5.8	40	7
CoFe/C	2.15	-44.6	2.15	5.5	60	8
Fe/Co/C nanocomplex	2.0	-54.6	2.5	8.8	33	1
PB@MoS_2	2.1	-42.84	2.4	7.31	40	9
CoFe/C(ZIF-67/PBA)	5.8	-44.1	2.3	5.2	60	10
FeCoNi alloy(FeCoNi-PBA)	1.91	-67	2.68	6.6	30	11
Core Shell NiCoFe/N-C	2.0	-57.5	2.0	5.44	-	12
Fe/Mn/C-800	2.3	-60.3	2.3	6.4	30	this work

References:

1 P. Miao, J. Chen, Y. Tang, K.-J. Chen and J. Kong, *Sci. China Mater.*, 2020, **63**, 2050-2061.

2 X. Wu, W. Ma, J. Xu, P. He, Y. Du, Y. Zhang, P. Zuo, H. Qi and Q. Zhuang, *ACS Appl. Nano Mater.*, 2022, **5**, 7300-7311.

3 X. Zeng, T. Nie, C. Zhao, G. Zhu, X. Zhang, R. Yu, G. D. Stucky and R. Che, *ACS Appl. Mater. Interfaces*, 2022, **14**, 41235-41245.

4 R. Qiang, Y. C. Du, H. T. Zhao, Y. Wang, C. H. Tian, Z. G. Li, X. J. Han and P. Xu, *J. Mater. Chem. A*, 2015, **3**, 13426-13434.

5 D. Liu, R. Qiang, Y. Du, Y. Wang, C. Tian and X. Han, *J. Colloid Interf. Sci.*, 2018, **514**, 10-20.

6 F. Y. Wang, N. Wang, X. J. Han, D. W. Liu, Y. H. Wang, L. R. Cui, P. Xu and Y. C. Du, *Carbon*, 2019, **145**, 701-711.

7 L. Cui, Y. Wang, X. Han, P. Xu, F. Wang, D. Liu, H. Zhao and Y. Du, *Carbon*, 2021, **174**, 673-682.

8 X. H. Liang, G. H. Wang, W. H. Gu and G. B. Ji, *Carbon*, 2021, **177**, 97-106.

9 Z. X. Zhao, S. W. Xu, Z. J. Du, C. Jiang and X. Z. Huang, *ACS Sustain. Chem. Eng.*, 2019, **7**, 7183-7192.

10 S. Wei, T. Chen, Q. Wang, Z. C. Shi, W. Li and S. G. Chen, *J. Colloid Interf. Sci.*, 2021, **593**, 370-379.

11 P. Li, Y. Zhao, Y. Zhao, J. Yan, H. Zhao, W. Zhao, J. Yun, C. Chen, Z. Deng and Z. Zhang, *Compos. Part B: Eng.*, 2022, **246**, 110268.

12 Y. J. Wang, Z. B. Pang, H. Xu, C. P. Li, W. J. Zhou, X. H. Jiang and L. M. Yu, *J. Colloid Interf. Sci.*, 2022, **620**, 107-118.